Optimizing thermo-mechanical processing and material coupling parameters in numerical modeling for additive manufacturing

Lamanna Antoine, Erwan Beauchesne, Pierre-Richard Dahoo, Constantin Meis

Optimizing thermo-mechanical processing and material coupling parameters in numerical modeling for additive manufacturing

Lamanna Antoine[1], Erwan Beauchesne[2], Dahoo Pierre-Richard[1] and Constantin Meis[3]
1 LATMOS/IPSL, UVSQ Université Paris-Saclay, Sorbonne Université, CNRS, 78280, Guyancourt, France
2 Altair Engineering, 5-10 Rue de la Renaissance, 92160 Antony, France
3 National Institute for Nuclear Science and Technology, CEA Saclay, 91191 Gif-sur Yvette, France
E-mail: lamanna.antoine@latmos.ipsl.fr, erwan.beauchesne@altair.com, francis@altair.com, pierre.dahoo@uvsq.fr, constantin.meis@cea.fr

Abstract
Additive manufacturing (AM) is gaining increasing industrial interest. Initially conceived to facilitate the pre-production, to manufacture efficiently and cheaply unique parts such as prototypes, it is now able to deliver parts that meet industrial production needs. In addition, AM is an effective way to achieve parts designed using topological optimization. Laser beam melting is an AM technique able to produce specific parts with mechanical properties matching industrial expectations. However, efficient production remains complex because of distortion, cracking and other failures linked to the process and to the machine parameters. The prime material being generally expensive and in order to achieve the required manufacturing quality from the very first attempt while reducing the processing time to market necessary for low cost mass production, a high-quality digital simulation is mandatory. We thus study the relation between the process and the material parameters with the final mechanical state of the part using a numerical model, which is developed in parallel.

This work focuses on the macroscopic scale. In order to carry out the thermo-mechanical study we use a finite element resolution method on the whole domain defined by the part, its supports and the baseplate. At this scale, one can neglect the packing of the powder as well as the hydrodynamic behavior of the melt pool in the laser beam melting process. We consider a Gaussian energy distribution for the heat source, imposed on several layers of powders below the deposited layer. Starting from a previous study [1], which considers the temperature dependence of the Young modulus, we improve, in this work, the model by considering the temperature dependency of other physical parameters pertaining to material properties or to elastoplastic and thermal laws coefficients. The aim is to bridge the macroscopic scale study of AM to the mesoscopic scale from results of this study.

In a first step, simulations are carried out with simple models like walls, cubes, beams and the popular cantilever used for calibrations. The results show the gain in precision with the contribution of the temperature dependence of various parameters as well as by considering the phase-transition during the printing process. The computing time is compatible with laptops and can iterate the simulations easily. The accuracy of the model is validated by comparing the distortion to the experimental results.

1. Introduction

Additive Manufacturing (AM) is becoming more and more relevant these days as it eases the pre-production, allows production of complex geometry parts, and manufacture cheaply but efficiently parts like prototypes. Several processes exist such as the Selective Laser Melting (SLM), Directed Metal Deposition (DMD) and Electron Beam Melting (EBM) and they all provide high quality and 99% dense parts. However, process control is uneasy and needs cycles of calibration. In addition, due to the large thermal gradients, defects like distortion and cracking can invalidate the part. Although

many studies have been carried out on this subject, it still remains a big challenge to master the process.

Trial and error cycles is a first approach to ensure that the printed part expected quality is reached. However, it is part-dependent and combined with the high powder cost, the effective number of trials is limited. Numerical simulation appears then as a valuable alternative. Design Of Experiment (DOE) is possible for free and gives much more freedom to designers. Besides the accuracy, the main issue is that the computation time must be smaller than the real printing time. A compromise between accuracy and computation times must therefore be found. Most of the industrial software now offers a range of accuracies starting from the lowest quality but fastest solution to the highest quality but slowest solution. Macroscopic scale modelling is considered to achieve the simulation of the whole part in an affordable time. At this scale, thermal and mechanical phenomena are both modelled to calculate the stress evolution and the distortion during and after the process. Melt pool phenomena are neglected as well as powder-laser interaction which is relevant at powder scale. This approach is also particularly helpful to the additional support structures which will act either as cooling channels either as reinforcement structures to minimize the part deformation.

Classical FE method is applied here for the simulation. The whole part is meshed with passive elements at the start. Material deposition is then modelled with elements active along the laser path. Two levels of activation are usually encountered in the literature: the quiet element method and the non-active element method [1]. In the former case, the physical properties of the elements have a limited impact on the construction region. In the latter case, these elements are not considered at all before being reached by the heat source. Detailed comparison of these two methods is given by Michaleris [2]. Beside elements management, the heat source is often model with the Goldak shape [2] used as in welding. Hodge et al. [5] used a model based on the radiation transfer equation proposed by Gusarov [4]. Another model, more suitable for ceramics, is based on the Beer-Lambert law as considered by Li et al. [6] and Chen et al. [7]. However, Chiumenti et al. [3] believes that a precise heat source distribution is not mandatory as the right amount of energy introduced in the heat affected zone is the most important parameter. Residual stress investigation was performed by Denlinger et al. [8] with a perfect elastoplastic model for Ti-6Al-4V using EBM. By introducing the stress relaxation, good agreement between measurement and simulation in distortion was achieved with appropriate relaxing temperature near to the start of the martensitic transformation. Zhang et al. [9] used elasto-viscoplastic model for SLM with IN718 alloy. Although the model was not yet validated thru experimental comparison, complex impeller was successfully simulated. Bugatti and Semerato et al. [10] investigated the inherent strain method, which consists in a residual plastic strain directly used in the simulation. They found better results with inherent strain taken from measurement than from meso-scale simulation.

In this work, an under-development simulation tool using finite element model for the simulation of additive manufacturing is used. This tool has already proven its capacity to accurately and quickly simulate the whole part. Several temperature dependant parameters were considered constant though. Therefore, the purpose here is to study the impact on the simulation’s precision when the temperature dependency is model for both the specific heat and the thermal conductivity of the material. At last, the laser scanning strategy will also be introduced as the influence of this parameter has been demonstrated experimentally [11].

2. Temperature dependency, specific heat and thermal conductivity

2.1. Equations

At the macroscopic scale, the heat source distribution is modelled with the energy deposition using a volumetric heat flow and a Gaussian distribution around the impact centre of the laser. This volumetric heat flow is computed considering the laser velocity, laser diameter and powder thickness.

$$E = \alpha . P . \Delta t \tag{1}$$

With:

α The powder absorption parameter

P The heating power

$$P = \phi . V_m \tag{2}$$

$$\phi = \frac{P_{laser}}{D_{laser} e_{powder}} \tag{3}$$

ϕ is the laser power per unit volume

Δt The interaction time between laser and power

$$\Delta t = \beta \frac{D_{laser}}{V_{laser}} \tag{4}$$

e_{powder} the powder thickness

β a proportionality factor (between 0 excluded and 1)

We do not consider the heat convection phenomena occurring in the melt pool which is not modelled in its liquidus state.

To properly write the energy balance at the macroscopic scale, we consider the unit volume of matter V. Inside this volume, we can write the energy balance equation:

$$E_{in} - E_{out} + E_{generate} = E_{accumulate} \tag{5}$$

At this scale, Fourier's law allows the density vector of entering thermic flow to be written as:

$$\varphi = -k(T) \nabla T \tag{6}$$

The thermal power accumulated is written as follows:

$$E_{acc} = V . \rho(T) . C_p(T) . \frac{\partial T}{\partial t} \tag{7}$$

Considering q, the heating source generated by this volume, we could naturally write:

$$E_{generate} = qV \tag{8}$$

To obtain the expression of the outcoming energy flow, we can write on every face ds, of this volume, the thermal power through ds along the normal n as:

$$d\varphi = \varphi \, ds \, . n \tag{9}$$

Therefore, decomposing under the x, y, z directions in the cartesian system:

$$E_{in}(u) - E_{out}(u) = \varphi(u + du) ds \, . n - \varphi(u) ds \, . n \text{ with u } = \text{ x, y, z} \tag{10}$$

Dividing (10) by the volume and making this volume tend to 0, we can write:

$$lim_{\Delta V \to 0} \frac{phi(u+du)\ ds\ .n\ -\ phi(u)\ ds\ .n}{\Delta V} = \frac{\partial phi_u}{\partial u} \tag{11}$$

Finally, reporting (11) in (10):

$$-\frac{\partial phi_x}{\partial x} - \frac{\partial phi_y}{\partial y} - \frac{\partial phi_z}{\partial z} + q = \rho(T).C_p(T)\frac{\partial T}{\partial t} \tag{12}$$

Replacing φ by its expression in (12), we can finally write the thermal energy conservation's equation:

$$\frac{\partial\left(k(T).\frac{dT}{dx}\right)}{\partial x} + \frac{\partial\left(k(T).\frac{dT}{dy}\right)}{\partial y} + \frac{\partial\left(k(T).\frac{dT}{dz}\right)}{\partial z} + \dot{q} = \rho(T).C_p(T).\frac{\partial T}{\partial t} \tag{13}$$

$$\nabla\big(k(T).\nabla(T)\big) + \dot{q} = \rho(T).C_p(T).\frac{\partial T}{\partial t} \tag{14}$$

Then

$$\rho(T).C_p(T).\frac{\partial T}{\partial t} - \nabla\big(k(T).\nabla(T)\big) = \dot{q} \tag{15}$$

In order to solve this equation, we use the expression of the residual r(T):

$$\rho(T).C_p(T).\frac{\partial T}{\partial t} - \nabla\big(k(T).\nabla(T)\big) - \dot{q} = r(T) \tag{16}$$

The weak form is then obtained by multiplying the right and left side of this equation by the test function T* and by integrating over the volume as follows:

$$\iiint r(T).T^*dV = \iiint T^*.\left(\rho.C_p.\frac{\partial T}{\partial t} - \nabla\big(k\nabla(T)\big) - Qv\right)dV \tag{17}$$

$$\iiint r(T).T^*dV = \iiint T^*.\rho.C_p.\frac{\partial T}{\partial t}dV - \iiint T^*.QvdV - \iiint T^*.\nabla\big(k\nabla(T)\big)dV \tag{18}$$

The Ostrogradski theorem applied on the product $T^*.\nabla\big(k\nabla(T)\big)$ gives

$$\iiint T^*.\nabla\big(k\nabla(T)\big)dV = \oiint T^*.q(T)dS - \iiint \nabla T^*.k\nabla T dV \tag{19}$$

Then if we implement (18) inside (17) we have:

$$\iiint r(T).T^*dV = \iiint T^*.\rho.C_p.\frac{\partial T}{\partial t}dV - \iiint T^*.QvdV - \oiint T^*.q(T)dS + \iiint \nabla T^*.k\nabla T dV \tag{20}$$

To solve this equation defined on the continuum we use a finite element method (FE). The temperature field is then linearly interpolated on each element as follows:

$$\{T\} = T(x,y,z,t) = \{N^e(x,y,z)\}.\{T^e(t)\} \tag{21}$$

$$\{\dot{T}\} = \dot{T}(x,y,z,t) = \{N^e(x,y,z)\}.\{\dot{T}^e(t)\} \tag{22}$$

With:

$\{T^e\}$ the nodal temperature vector for an element e
$\{N^e\}$ The interpolation function vector for an element e
$[B_e] = \nabla[N_e]$

We can then write the discrete problem:

$$\sum_e \rho . C_p \left(\iiint [N_e]^t [N_e] dV_e \right) \frac{d\{T^e\}}{dt} + \sum_e \left(\iiint k(T) . [B_e]^t [B_e] dV_e \right) \{T^e\} = \left(\sum_e \iiint [N_e] Q_v dVe + \sum_e \oiint [N_e] . q(T) dS \right) \quad (23)$$

Which is a differential non-linear equations system:

$$[C]\{\dot{T}\} + [K]\{T\} = \{F\} \quad (24)$$

With:

$$[C] = \rho . C_p . \sum_e \iiint [N_e]^t [N_e] dV_e$$

$$[K] = \sum_e \left(\iiint k(T) . [B_e]^t [B_e] dV_e \right)$$

$$\{F\} = \sum_e \left(\iiint [N_e] Q_v dVe + \oiint [N_e] . q(T) dS \right)$$

This can be solved using classical numerical methods and considering the appropriate time scheme.

3. Influence of the strategy used to simulate the printing.

As we see in this work, the deposition model works with element activation technique. The initial geometry is meshed so that the elements are organized in layers along z direction. To ensure the meshing robustness, element distribution in layers, and numerical stability, both full integrated elements and voxel mesh are used.

At the beginning of the simulation all the elements are deactivated and then activated when reached by the laser beam. The three strategies we'll use in this work are the so call 'by-layer' and the 'by-hatch' activation. In the former, the whole layer elements are activated at the same time whereas in the latter, these elements are activated by group in a time sequence.

The time sequences are also different. In the "by-later' approach, the time between two layers activation is the time the laser would take to scan the entire layer plus the powder recoating time. For the 'by hatch' strategy, the time between two hatches activation is the time the laser would take to scan the entire hatch. A temporality is then introduced within the layer activation itself. This activation time is also much smaller than the one between two layers activation in the former approach which will explain the difference in the results.

The 'by layer' strategy which has already shown good correlation with experimental measurements [11] will be used as a reference to evaluate the gain of accuracy with the 'by-hatch' scanning strategy.

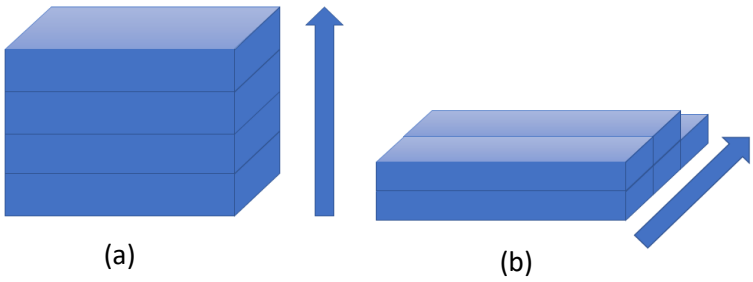

Figure 1. Element activation strategies: (a) By layer in printing direction Z; (b) by hatch in printing direction X or Y direction

4. Results

The first results are given for a 10x10x10 mm cube. The purpose is to quickly illustrate the difference between the element activation strategies and the parameters considered.

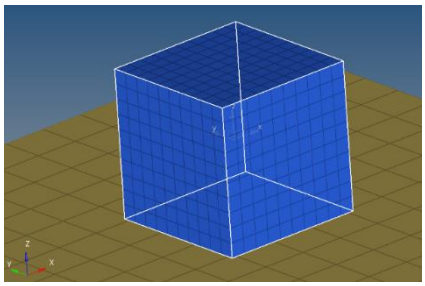

Figure 2. 10x10x10 mm cube model.

Then to validate our approach we'll use the bridge model for which the experimental measurement of the angle for different scanning strategies are given in [13]. A bridge is built on a plate then cut off from this plate. The resulting spring-back effect is then measured thru the angle between the bottom surfaces of the two bridge's pillar. This is the so call Bridge Curvature Method (BCM).

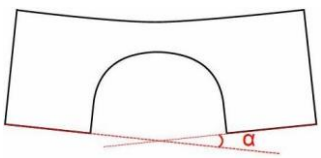

Figure 3. Measured angle α.

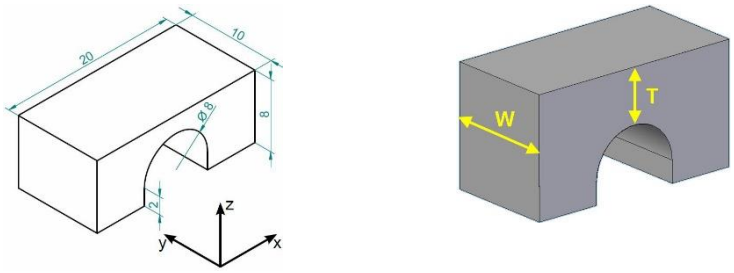

Figure 4. Dimensions of the bridge as described by Kruth [13]

The dimensions of the bridge are given in Kruth's paper [13], with a width [W] of 10mm and a thickness [T] of 2mm. We'll consider titanium Ti-6Al-4V as the material.

Table 1. Reference parameters used to build Ti-6Al-4V test parts on the KUL-SLM machine.

Material	Ti-6Al-4V
Hatch spacing	74 µm
Scan speed	225 mm/s
Laser power	42 W
Contour scan	before fill
Layer thickness	30 µm
Reference value	$\alpha_{ref,\,LM}$ = 2,797°± 0,033°

4.1. Temperature dependency of the thermal conductivity

We apply the "by layer" approach described above on a hundred of elements cube. The temperature dependency of both the thermal conductivity and the specific heat for the TIA6V are given in Yannick Robert's works [12].

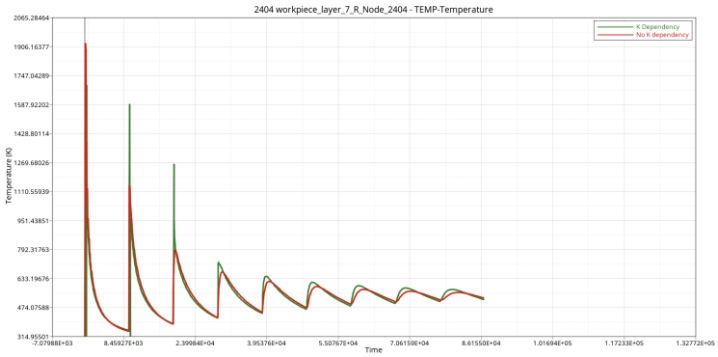

Figure 5. Comparison of the temperature with and without temperature dependency for thermal conductivity on a 10x10x10 mm cube of Tia6v.

We can observe that the first temperature peak is the same with and without the temperature dependency. The differences appear from the second peak. This can be explained by the higher conductivity of the previously activated layers, when the temperature dependency is set, which are re-heated at each new above layer activation. The heat flow between two consecutive layers is then higher from the top one to the bottom one. Due to this higher conductivity the cooling rate is then faster which can be observed on the decreasing slop of the curve after each peak.

4.2. Scanning path

We first use here the same cube model to highlight the difference between the two approaches.

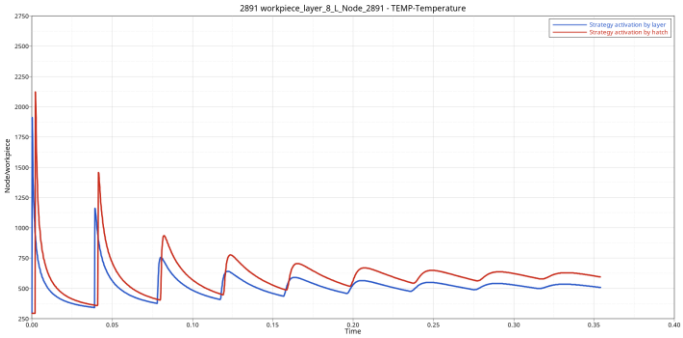

Figure 6. Comparison of the temperature depending on the scanning strategy on a 10x10x10 cube.

As shown in Figure 5, the heat peaks are slightly higher with the activation 'by hatch' than 'by layer'. This can be explained by the shorter time between two sequences of activation for the former strategy as explained in the chapter 2. The previously activated elements are still at a high temperature when the next range of elements is activated which was not the case for the "by layer" strategy. As a result, the maximum temperature reached is also higher for the "by hatch" strategy.

Table 2. Maximal temperature depending on the strategy for Tia6v on 10x10x10 cube

	Tmax (K)
By Layer	1911
By Hatch /X	2122

Using the BCM, we can compare the angle given by the simulation with the experimental values. As shown in Figure 7 the precision earned depends of both the orientation and of the strategy. We can observe that the accuracy of the "by layer" strategy is not improved by the temperature dependency of the specific heat and the conductivity whereas the gain for the "by hatch" strategy rises to 12%. This modelling is not fine enough to capture this level of details. Although this latter is still coarse regarding a real laser scanning path, it introduces a temporality in the temperature evolution within each layer which doesn't exist for the "by layer" strategy.

Table 3. Comparison of alpha angle depending on the strategy

Scanning strategy	Reference	Tia6v without dependency	Tia6v with dependency	Difference in % between with and without temperature dependency
By layer	2.797	2.841	2.945	-3.7
90°	1	1.3	1.1775	+12.3
0°	2.797	2.723	2.73	+0.25

Figure 7. Comparison between the calculated angle, depending on the strategy used and if the parameters depending on the temperature, and the reference.

5. Conclusion

In this work, a macroscopic model for the thermo-mechanical simulation of additive manufacturing has been developed. Thermal dependency of specific heat and conductivity parameters has been added. Element activation/deactivation technique is used. Two element activation strategies have been studied. The BCM method was used and gave good results for the Tia6v material for the two scanning strategies at 0° and 90°. Thanks to this work, the cooling history is considered much more precisely in the simulation, preparing the introduction of phase change models for which the cooling rate is a first order parameter. We also demonstrate that a more realistic element activation sequence improve a lot the results. This will have to be again enhanced in future works. Besides, meso-scale modelling will be also explored to better calibrate the heating energy which makes sense as we'll model in more details the laser path.

6. References

[1] Lindgren L-E and Hedblim E, Commun. Num. Meth. Eng., 17(9), 647-57
[2] Michaleris P, Fin. Elem. Anal. Des., 86, 51-60
[3] Chiumenti M, Neiva E, Salsi E, Cervera M, Badia S, Moya J, Chen Z, Lee C and Davies C, Commun. Num. Meth. Eng., 18, 171-85
[4] Gusarov A V and Kruth J-P, Int. J. Heat Mass Trans., 48(16), 3423-34
[5] Hodge N E, Ferencz R M and Solberg J M, Appl. Surf. Sci., 254(4), 975-9
[6] Li J F, Li L and Stott F H, Int. J. Heat Mass Trans., 47(6-7), 1159-74
[7] Chen Q, Guillemot G, Gandin Ch-A and Bellet M, Add. Manu., 16, 124-37
[8] Denlinger E R, Heigel J C and Michaleris P, Proc. Inst. Mech. Eng., B: J. Eng. Manu., 229(10), 1803-13
[9] Zhang Y, Guillemot G, Bernacki M and Bellet M, Comp. Meth. Appl. Mech. Eng., 331, 514-35
[10] Bugatti M and Semerato Q, Add. Manu., 23, 329-46
[11] Chen Q., Beauchesne E., Arnaudeau F., Dahoo P.-R., Meis C., Model. of mech. behave. in add. manuf. at part scale, J. of Physics: Conf. Series, Vol. 1391, 8th Int Conf. on Math. Model. in Phys. Science 26–29 Aug. 2019, Bratislava, Slovakia

[12] Robert Y., Sim. num. du soud. du ta6v par laser yag impuls. Phd Thesis. Sept 2007. Ecole Des Mines-Paritech
[13] Kruth J-P, Deckers J., Yasa E., Wauthlé R., Assess. and compar. Influenc. Fac. of res. stresses in S.L.M. Proceedings of the Institution of Mechanical Engineers Part B Journal of Engineering Manufacture (P I MECH ENG B-J ENG)